

Hardness, elastic, and electronic properties of chromium monoboride

Lei Han, Shanmin Wang, Jinlong Zhu, Songbai Han, Wenmin Li, Bijuan Chen, Xiancheng Wang, Xiaohui Yu, Baochang Liu, Ruifeng Zhang, Youwen Long, Jinguang Cheng, Jianzhong Zhang, Yusheng Zhao, and Changqing Jin

Citation: *Applied Physics Letters* **106**, 221902 (2015); doi: 10.1063/1.4922147

View online: <http://dx.doi.org/10.1063/1.4922147>

View Table of Contents: <http://scitation.aip.org/content/aip/journal/apl/106/22?ver=pdfcov>

Published by the AIP Publishing

Articles you may be interested in

Elastic anisotropy and shear-induced atomistic deformation of tetragonal silicon carbon nitride

J. Appl. Phys. **116**, 023509 (2014); 10.1063/1.4889931

Hardness and incipient plasticity in silicate glasses: Origin of the mixed modifier effect

Appl. Phys. Lett. **104**, 051913 (2014); 10.1063/1.4864400

Experimental verification and theoretical analysis of the relationships between hardness, elastic modulus, and the work of indentation

Appl. Phys. Lett. **92**, 231906 (2008); 10.1063/1.2944138

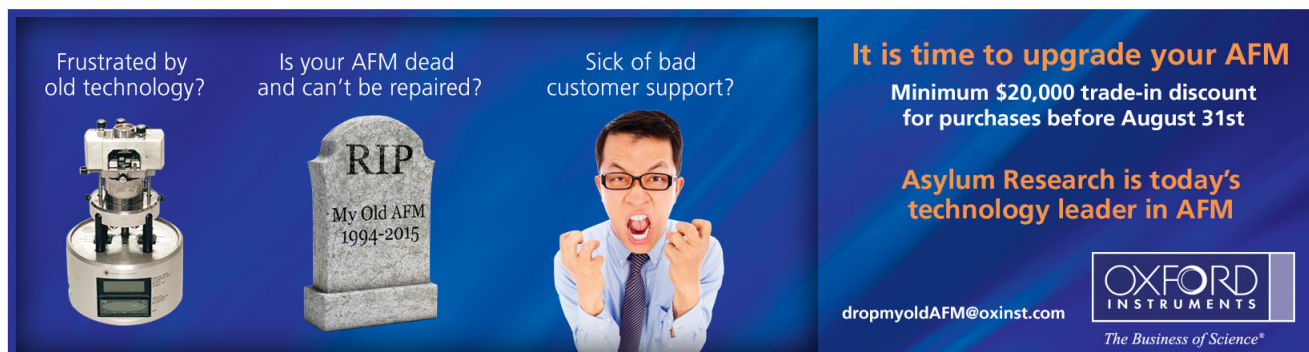
Ground-state properties and hardness of high density B C 6 N phases originating from diamond structure

J. Appl. Phys. **101**, 083505 (2007); 10.1063/1.2723866

Elastic and mechanical properties of transparent nanocrystallized KNbGeO 5 glass

J. Appl. Phys. **94**, 5265 (2003); 10.1063/1.1609641

Frustrated by old technology? Is your AFM dead and can't be repaired? Sick of bad customer support?



It is time to upgrade your AFM
Minimum \$20,000 trade-in discount for purchases before August 31st

Asylum Research is today's technology leader in AFM

dropmyoldAFM@oxinst.com

OXFORD INSTRUMENTS
The Business of Science®

Hardness, elastic, and electronic properties of chromium monoboride

Lei Han,^{1,2} Shanmin Wang,³ Jinlong Zhu,³ Songbai Han,⁴ Wenmin Li,¹ Bijuan Chen,¹ Xiancheng Wang,¹ Xiaohui Yu,^{1,a)} Baochang Liu,^{2,a)} Ruifeng Zhang,^{5,a)} Youwen Long,¹ Jinguang Cheng,¹ Jianzhong Zhang,⁶ Yusheng Zhao,^{1,3} and Changqing Jin¹

¹Beijing National Laboratory for Condensed Matter Physics and Institute of Physics, Chinese Academy of Sciences, Beijing 100190, China

²College of Construction Engineering, Jilin University, Changchun, Jilin 130061, China

³HiPSEC and Department of Physics, University of Nevada, Las Vegas, Nevada 89154, USA

⁴Neutron Scattering Laboratory, China Institute of Atomic Energy, Beijing 102413, China

⁵School of Materials Science and Engineering, Beihang University, Beijing 100191, China

⁶LANSCe Division, Los Alamos National Lab, Los Alamos, New Mexico 87545, USA

(Received 10 April 2015; accepted 23 May 2015; published online 3 June 2015)

We report high-pressure synthesis of chromium monoboride (CrB) at 6 GPa and 1400 K. The elastic and plastic behaviors have been investigated by hydrostatic compression experiment and micro-indentation measurement. CrB is elastically incompressible with a high bulk modulus of 269.0 (5.9) GPa and exhibits a high Vickers hardness of 19.6 (0.7) GPa under the load of 1 kg force. Based on first principles calculations, the observed mechanical properties are attributed to the polar covalent Cr-B bonds interconnected with strong zigzag B-B covalent bonding network. The presence of metallic Cr bilayers is presumably responsible for the weakest paths in shear deformation. © 2015 AIP Publishing LLC. [<http://dx.doi.org/10.1063/1.4922147>]

Transition-metal borides (TMB) have been extensively studied over the past decades because of their high hardness, excellent corrosion resistance, and relatively high electrical conductivity.^{1–3} As commonly accepted, the high hardness is attributed to strong directional covalent bonds between the TM and the light elements boron.^{4,5} The high valence-electron density in transition metals is responsible for the high value of bulk modulus under hydrostatic pressure, while the introduction of light elements such as boron can significantly increase the resistance to plastic shear due to the formation of strong covalent metal-boron and boron-boron bonding networks.⁵

Because metallic bonds in TMB may induce the lattice softening under shear deformation, much effort has been made to increase the shear plastic resistance by incorporating high boron content to form three dimensional (3D) networks of covalent bonds. Consequently, a series of diborides and tetraborides of transition metals have been synthesized and investigated by both experiments and theoretical calculations.^{6–11} Of the transition metal diborides, OsB₂,⁶ RuB₂, and ReB₂⁷ are typical examples that can be synthesized at ambient pressure. OsB₂ possesses high elastic moduli but a low hardness due to the presence of weak metallic bonds.¹² ReB₂ was believed to be superhard,¹³ but the measured asymptotic hardness (i.e., load-independent) is less than 30 GPa because of the electronic instabilities of 5*d* orbitals under finite shear strain, which results in transformation to phases with lower plastic resistance.¹⁴ Since Os, Ru, and Re are all noble metals, the high cost of these materials will also hinder their large scale production and a broad application in industry.

Transition metal tetraborides, TMB₄, are promising candidates of ultraincompressible and hard materials. In general,

higher boron content incorporates additional B-B covalent bonds, which would in principle lead to improved hardness. This correlation, although currently still under debate, appears to hold well for some tetraborides such as WB₃ (originally reported as WB₄),⁸ FeB₄,⁹ and CrB₄,^{10,11} all of which exhibit superior mechanical properties. Besides intrinsic mechanical properties, synthesis condition is another factor that must be considered because the current techniques for the synthesis of TMB₄ require either very high temperature such as arc melting or extreme pressure conditions. For massive and industrial-scale production, the use of earth-abundant and inexpensive materials along with modest synthesis P-T conditions is highly desired. Tungsten monoboride, WB, which can be synthesized under 3 GPa and 1000 °C and exhibits a high hardness of ~28 GPa,¹⁵ is a good example of ultraincompressible and hard materials based on transition metal monoboride.

In this letter, we studied systematically the hardness and elastic and electrical properties of monoboride CrB, by means of experiments and first principles calculations. The observed mechanical behaviors are found to be closely related to the formation of polar Cr-B bonds interconnected with strong zigzag B-B covalent bonds in the crystal structure of CrB. The presence of Cr-Cr bimetallic layers should provide a unique combination of metal and ceramic properties.

Commercially available crystalline powders of Cr (>99.9% pure) and B (>99.5% pure) in a molar ratio Cr:B = 1:1.05 were homogeneously mixed for the synthesis of CrB. In each experimental run, a pre-pressed pellet was placed in an MgO capsule, which was then sealed in a graphite heater. High-P experiments were performed in a DS 6 × 600 T cubic press. At the target pressure of 6 GPa, the temperature was gradually increased to 1400 K at a heating rate of 360 K/min, and the sample was soaked for 15 min before quenching to room temperature. After turning off the

^{a)}Authors to whom correspondence should be addressed. Electronic addresses: yuxh@iphy.ac.cn; liubc@jlu.edu.cn; and zrf@buaa.edu.cn.

electric power, the sample temperature can be rapidly dropped under 373 K in 60 s because the anvils are surrounded by the cooling water tubing.

The final products were characterized by x-ray diffraction with Cu K α radiation. The crystal structure was refined based on XRD data using Rietveld refinements and the GSAS software.¹⁶ The Vickers hardness was measured using a micro-hardness tester on well-sintered bulk samples under different applied loads of 10–1000 g. Under each load, the measurement was repeated 10 times with a dwelling time of 15 s, and the reported Vickers hardness is the mean value of 10 data points. The uncertainty σ is calculated from: $\sigma = \sqrt{\frac{1}{N} \sum_{i=1}^N (x_i - \bar{x})^2}$, where $N=10$ in our case, x_i is the hardness value from each individual indentation, and \bar{x} is the mean value of the measured hardness.

High-P synchrotron x-ray diffraction experiments using a diamond-anvil cell (DAC) were performed at the Beijing Synchrotron Radiation Facility (BSRF), China. The obtained boride was ground into powders and loaded into the sample hole in a stainless steel gasket with neon as pressure-transmitting medium. A few ruby balls were also loaded into the same sample chamber to serve as internal pressure standard. The collected angle-dispersive diffraction data were analyzed by integrating 2D images as a function of 2θ using the program Fit2D to obtain conventional, one-dimensional diffraction profiles.¹⁷

Figure 1(a) shows the crystal structure of CrB with space group of Cmc m (No. 63) refined from XRD pattern. The detail refined lattice parameters and atom positions are in good agreement with Ref. 18, and listed in Table S1.¹⁹ The refined XRD patterns are shown in Figure S1.¹⁹ As shown in Figure 1(a), each Cr atom is surrounded by seven B atoms with three type denoted as B1, B2, and B3. The B1 atoms, which form a tetragonal plane parallel to the a - c plane, are closest to Cr atoms with a distance of ~ 2.19 Å, representing the strongest bonding between the Cr and B atoms. Cr-B2 and Cr-B3 bonds have longer distances of ~ 2.22 Å and 2.29 Å, respectively, suggesting that weaker interactions. On the other hand, the B1-B2 bonds form zigzag boron chains with a bonding distance of ~ 1.78 Å in the b - c plane, which is much shorter than that in WB.^{15,20} This may play an important role in resisting the plastic deformation.

Phase stability and compressibility of CrB were investigated by synchrotron x-ray diffraction in a DAC. Figure 1(b) shows selected XRD patterns collected under room-temperature compression. The orthorhombic CrB is structurally stable up to 16 GPa and no phase transition was observed. The derived pressure-volume data for CrB are fitted to the second order Birch-Murnaghan equation of state²¹ as shown in Figure 1(c), and the obtained bulk modulus, B , is 269.0 (5.9) GPa. Figure S2 shows the relative cell parameters as a function of pressure;¹⁹ CrB displays more nearly isotropic compressibility compared to CrB₂.¹¹ As expected, the c -axis is slightly less compressible than the a and b axes because the zigzag boron-boron chains are primarily along the c direction. While along the a and b directions, the axial compressibility is mainly determined by the strength of Cr-B and Cr-Cr bonds.

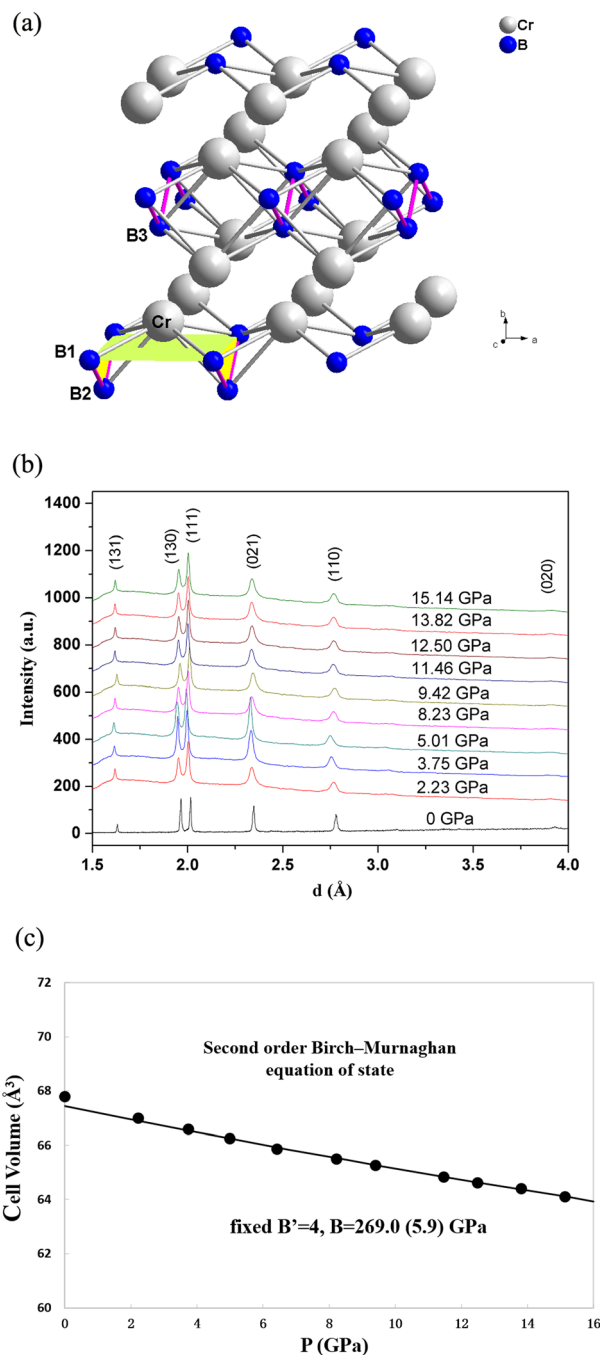


FIG. 1. (a) The crystal structure of orthorhombic CrB. (b) High-pressure XRD patterns collected at room temperature, (c) the volume-pressure data fitted to the 2nd order Birch-Murnaghan equation of state.

The density of the sintered pellet was measured by using the Archimedes method. The measured density is ~ 5.4 g/cm³, which is $\sim 89\%$ of the theoretical density (~ 6.1 g/cm³), indicating that a small amount of porosity and/or unreacted boron may be present in the sintered sample, the latter of which is insensitive to x-ray diffraction measurement. The Vickers hardness measurements were performed on the bulk sample. As shown in Figure 2, the determined asymptotic hardness of CrB is ~ 19.6 (0.7) GPa, which is comparable to that of the well-known WC and OsB₂. However, CrB shows higher hardness over CrB₂ (16 GPa under the load of 500 g),¹¹ indicating that the boron content is not necessarily a determining factor for the design of hard and superhard materials. As will be discussed later in the paper,

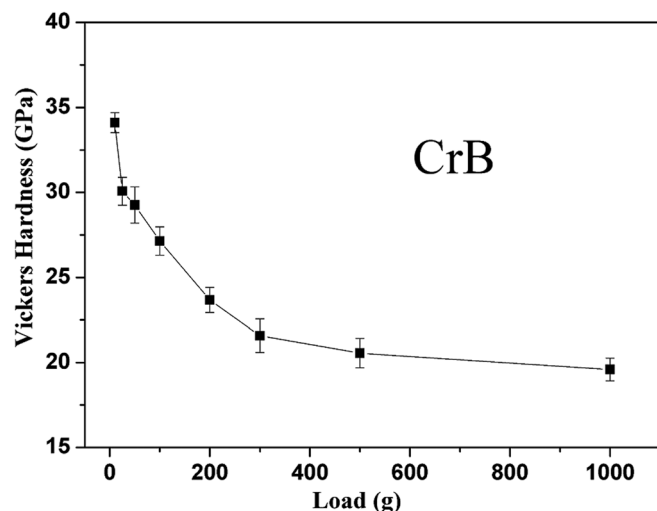


FIG. 2. Measured Vickers hardness as a function of applied loads from 10 g to 1000 g.

the enhanced mechanical behavior of CrB is mainly attributed to the strong 3D Cr-B and zigzag B-B bonding networks.

Figure S3 shows a typical electrical resistivity-temperature curve of metallic behavior of CrB.¹⁹ The resistivity at room temperature is about $2.3 \mu\Omega \text{ m}$, comparable to some metal alloy. The resistivity decreases linearly with decreasing temperature in the range of 300–60 K, and then flattens out and approaches a plateau value of $0.4 \mu\Omega \text{ m}$ as temperature further decreases to 2 K. The upturn of resistivity at low temperatures due to the Kondo effect was not observed, suggesting that the scattering of conduction electrons due to magnetic impurity is negligibly weak. The data from 2 to 60 K are fitted by a formula $\rho = \rho_0 + AT^n$, where ρ_0 is the residual resistivity, and the observed data can be well described by $\rho_0 = 0.4 \mu\Omega \text{ m}$ and $n = 2.7$. The residual resistivity ratio RRR, defined as $\rho(300 \text{ K})/\rho_0$, is 5.7, which is very small for the large contribution of impurity (extra boron) or grain boundary to the resistivity.

First principles calculations were performed using the VASP code with the generalized-gradient approximation proposed by Perdew and Wang for exchange-correlation functional.²² The optimized lattice constants of orthorhombic CrB (referred as oS8 later in the manuscript, $a = 2.925 \text{ \AA}$, $b = 7.839 \text{ \AA}$, $c = 2.915 \text{ \AA}$, listed in Table I) are in good agreement with the experimental results and previous Density Functional Theory (DFT) calculations.²⁰ Meanwhile, single-crystal elastic constants of CrB were calculated using the efficient strain-energy method.²³ The obtained elastic constants of oS8 are listed in Table S2. By means of the Voigt averaging method, we obtained the Voigt bulk modulus $B_V = 304.8 \text{ GPa}$, shear modulus $G_V = 225.4 \text{ GPa}$, and Poisson

TABLE I. Experimental and simulated results of lattice parameters, bulk modulus, shear modulus, and Poisson's ratio of orthorhombic (No. 63) and tetragonal (No. 141) phase CrB.

CrB	a (Å)	b (Å)	c (Å)	B (GPa)	G (GPa)	ν
Experiment	2.959	7.846	2.919	269.0		
oS8	2.925	7.839	2.915	304.8	225.4	0.203
tI16	2.919		15.673	306.4	230.5	0.199

ratio $\nu = 0.203$. The Voigt bulk modulus from simulation is comparable to our experiment value $\sim 269 \text{ GPa}$. In addition, the tetragonal phase of CrB (referred as tI16 later) was also calculated for comparison, and the calculated results are summarized in Tables I and S2. Surprisingly, even with different crystal structures and compliance parameters, the oS8 and tI16 CrB phases show very similar bulk modulus and shear modulus. The calculated shear moduli are even comparable to hard ReB_2 and WB_3 ,²⁴ indicating that they have similar shear stiffness.

In order to gain deeper understanding into the mechanical properties of oS8 and tI16-CrB, the orbital decomposed electronic density of states (DOS) is calculated and shown in Figure 3. It is found that both CrB phases show finite DOS at the Fermi level and hence exhibit metallic behavior. Another important feature in Figure 3 is the presence of the so-called “pseudo-gap” for tI16-CrB, which is the difference between the bonding and anti-bonding states. This suggests a strong “pseudo-covalent” contribution due to the hybridization between Cr d orbital and B p orbital. However, the “pseudo-gap” does not exist in oS8-CrB, indicating that the oS8 phase should exhibit a conventional metallic-type electrical conductivity, consistent with the experimental results discussed above. Figure 4 shows the bond structures and isosurface of the valence charge density difference (VCDD) of tI16 and

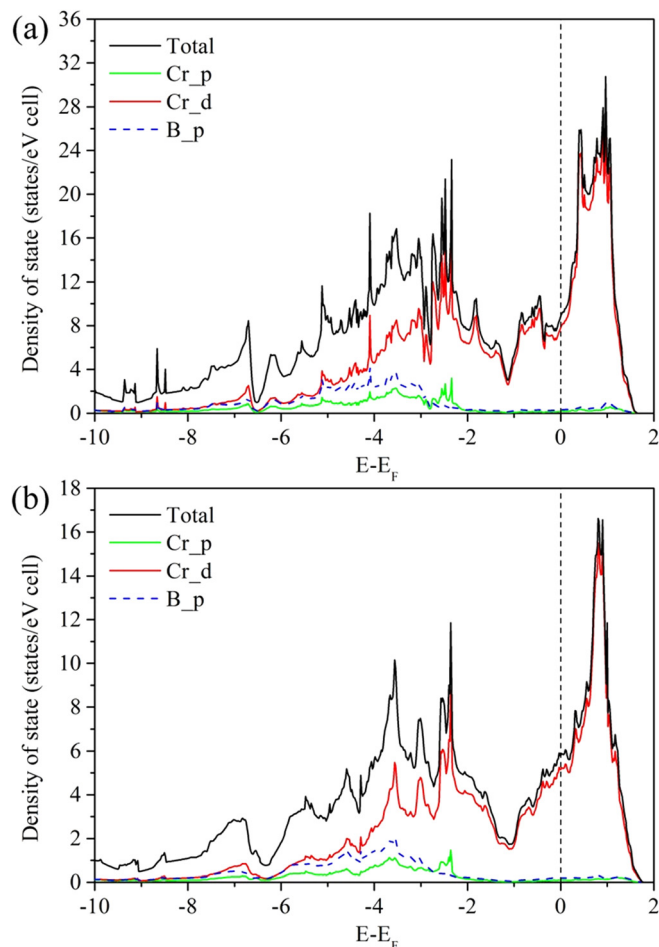


FIG. 3. Partial density of states for (a) tI16-CrB and (b) oS8-CrB. The red solid and blue dashed curves are from Cr d orbital and B p orbitals, respectively. The vertical dashed lines indicate the Fermi level.

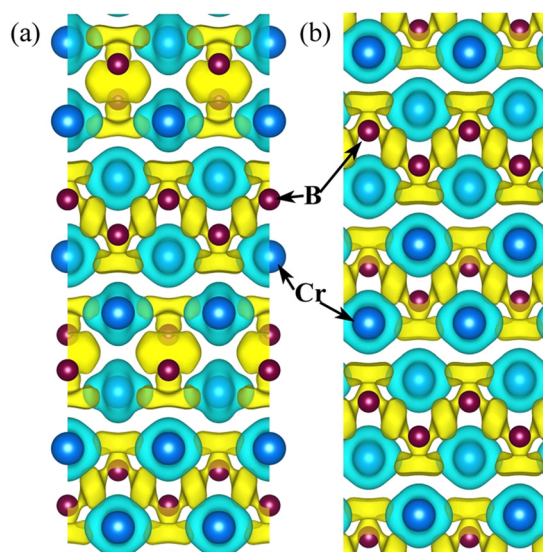


FIG. 4. The isosurface maps of VCDD of (a) tI16-CrB and (b) oS8-CrB. The large blue and small red spheres represent Cr and B atoms, respectively. The yellow color bounded regions indicate the formation of covalent bonding networks due to charge accumulation.

oS8-CrB. The polar covalent Cr-B bonds and strong B-B directional covalent bond networks in the CrB structure can be clearly identified from the electron localization/transfer maps shown in Figure 4. The yellow colored Cr-B and B-B bonds indicate the contribution of covalent bonding due to charge accumulation. Such high electronic partition should presumably be responsible for the high bulk and shear modulus values observed in CrB. However, the presence of metallic Cr bilayers (see Figure 4) is expected to weaken the shearing paths in a similar manner to what has been shown in OsB₂.²⁵ Nevertheless, the Cr bilayers may also provide a unique combination of metal and ceramic properties for CrB as shown in Figure 3.

In summary, we synthesized orthorhombic CrB at high P-T conditions of 6 GPa and 1400 K through solid-state reaction between chromium and boron elements. The elastic compressibility of CrB was studied in DAC up to 16 GPa at room temperature, and the obtained bulk modulus from the second order Birch-Murnaghan equation of state is higher than those of CrB₂ and CrB₄. In addition, the Vickers hardness of ~20 GPa under the load of 1 kg is higher than that of CrB₂, indicating that the monoborides can have better mechanical performance than the diboride counterparts. The boron content is hence not a necessary criterion for the design of hard and superhard materials. First principle simulation reveals that the symmetrical electronic partition of the 3D Cr-B and zigzag B-B bonding networks should be responsible for its high values of bulk and shear moduli. However,

the presence of metallic Cr bilayers would be responsible for the weakest shearing paths in a similar manner to that shown in WB₃.

High pressure synchrotron x-ray experiments in a diamond-anvil cell (DAC) were performed at Beijing Synchrotron Radiation Facility (BSRF), China. This research was supported by CNSF under Contract Nos. 51402350 and 51471018. RFZ thanks to the Fundamental Research Funds for the Central Universities of Beihang University.

¹S. Veprek, R. F. Zhang, and A. S. Argon, *J. Superhard Mater.* **33**, 409 (2011).

²E. Zhao, J. Meng, Y. Ma, and Z. Wu, *Phys. Chem. Chem. Phys.* **12**, 13158 (2010).

³W. G. Fahrenholtz, G. E. Hilmas, I. G. Talmy, and J. A. Zaykoski, *J. Am. Ceram. Soc.* **90**, 1347 (2007).

⁴R. B. Kaner, J. J. Gilman, and S. H. Tolbert, *Science* **308**, 1268 (2005).

⁵J. B. Levine, S. H. Tolbert, and R. B. Kaner, *Adv. Funct. Mater.* **19**, 3519 (2009).

⁶R. W. Cumberland, M. B. Weinberger, J. J. Gilman, S. M. Clark, S. H. Tolbert, and R. B. Kaner, *J. Am. Chem. Soc.* **127**, 7264 (2005).

⁷J. B. Levine, S. L. Nguyen, H. I. Rasool, J. A. Wright, S. E. Brown, and R. B. Kaner, *J. Am. Chem. Soc.* **130**, 16953 (2008).

⁸R. Mohammadi, A. T. Lech, M. Xie, B. E. Weaver, M. T. Yeung, S. H. Tolbert, and R. B. Kaner, *Proc. Natl. Acad. Sci. U.S.A.* **108**, 10958 (2011).

⁹H. Gou, N. Dubrovinskaia, E. Bykova, A. A. Tsirlin, D. Kasinathan, W. Schnelle, A. Richter, M. Merlini, M. Hanfland, A. M. Abakumov, D. Batuk, G. V. Tendeloo, Y. Nakajima, A. N. Kolmogorov, and L. Dubrovinsky, *Phys. Rev. Lett.* **111**, 157002 (2013).

¹⁰A. Knappschneider, C. Litterscheid, D. Dzivenko, J. A. Kurzman, R. Seshadri, N. Wagner, J. Beck, R. Riedel, and B. Albert, *Inorg. Chem.* **52**, 540 (2013).

¹¹S. Wang, X. Yu, J. Zhang, Y. Zhang, L. Wang, K. Leinenweber, H. Xu, D. Popov, C. Park, W. Yang, D. He, and Y. Zhao, *J. Superhard Mater.* **36**, 279 (2014).

¹²J. Yang, H. Sun, and C. F. Chen, *J. Am. Chem. Soc.* **130**, 7200 (2008).

¹³H. Y. Chung, M. B. Weinberger, J. B. Levine, A. Kavner, J. M. Yang, S. H. Tolbert, and R. B. Kaner, *Science* **316**, 436 (2007).

¹⁴R. F. Zhang, D. Legut, R. Niewa, A. S. Argon, and S. Veprek, *Phys. Rev. B* **82**, 104104 (2010).

¹⁵Y. Chen, D. He, J. Qin, Z. Kou, S. Wang, and J. Wang, *J. Mater. Res.* **25**, 637 (2010).

¹⁶B. H. Toby, *J. Appl. Cryst.* **34**, 210 (2001).

¹⁷A. P. Hammersley, S. O. Svensson, M. Hanfland, A. N. Fitch, and D. Hausermann, *High Pressure Res.* **14**, 235 (1996).

¹⁸P. Mohn and D. G. Pettofor, *J. Phys. C: Solid State Phys.* **21**, 2829 (1988).

¹⁹See supplementary material at <http://dx.doi.org/10.1063/1.4922147> for the refined XRD pattern, relative cell parameters as a function of pressure, and the electrical resistivity of CrB.

²⁰H. Gou, Z. Li, J. Zhang, H. Niu, F. Gao, R. C. Ewing, and J. Lian, *Comput. Mater. Sci.* **53**, 460 (2012).

²¹F. Birch, *Phys. Rev.* **71**, 809 (1947).

²²G. Kresse and J. Hafner, *Phys. Rev. B* **47**, 558 (1993).

²³R. F. Zhang, S. Veprek, and A. S. Argon, *Appl. Phys. Lett.* **91**, 201914 (2007).

²⁴R. F. Zhang, D. Legut, Z. J. Lin, Y. S. Zhao, H. K. Mao, and S. Veprek, *Phys. Rev. Lett.* **108**, 255502 (2012).

²⁵R. F. Zhang, D. Legut, X. D. Wen, S. Veprek, K. Rajan, T. Lookman, H. K. Mao, and Y. S. Zhao, *Phys. Rev. B* **90**, 094115 (2014).